



HAL
open science

Kinetic ellipsometry applied to soft X-ray multilayer growth control

Ph. Houdy

► **To cite this version:**

Ph. Houdy. Kinetic ellipsometry applied to soft X-ray multilayer growth control. *Revue de Physique Appliquée, Société française de physique / EDP*, 1988, 23 (10), pp.1653-1659. 10.1051/rphysap:0198800230100165300 . jpa-00245994

HAL Id: jpa-00245994

<https://hal.archives-ouvertes.fr/jpa-00245994>

Submitted on 1 Jan 1988

HAL is a multi-disciplinary open access archive for the deposit and dissemination of scientific research documents, whether they are published or not. The documents may come from teaching and research institutions in France or abroad, or from public or private research centers.

L'archive ouverte pluridisciplinaire **HAL**, est destinée au dépôt et à la diffusion de documents scientifiques de niveau recherche, publiés ou non, émanant des établissements d'enseignement et de recherche français ou étrangers, des laboratoires publics ou privés.

Classification

Physics Abstracts

05.20 — 41.10 — 72.10 — 73.10K

Kinetic ellipsometry applied to soft X-ray multilayer growth control

Ph. Houduy

Laboratoires d'Electronique et de Physique Appliquée (LEP) (*), 3 avenue Descartes, 94451 Limeil-Brévannes Cedex, France

(Reçu le 26 octobre 1987, révisé le 24 mai 1988, accepté le 26 mai 1988)

Résumé. — L'ellipsométrie est une méthode de caractérisation permettant la détermination des indices optiques et des épaisseurs des films minces. Nous avons utilisé cette méthode pour contrôler, durant le dépôt, la réalisation par pulvérisation diode RF de multicouches X. Trois paramètres limitent la réflectivité des multicouches : les défauts de compacité, les dérivés en épaisseur et les rugosités interfaciales. La précision de nos ellipsomètres étant de 0,1 Å sur l'épaisseur et de 10^{-3} sur l'indice optique, nous avons pu optimiser la qualité des dépôts, contrôler les vitesses de croissance et comprendre les mécanismes de formation des interfaces. Ceci nous a amenés à réaliser des optiques X de bonne qualité pour des longueurs d'onde inférieures à 44,7 Å. Nous avons ainsi réalisé des empilements carbone/tungstène de 200 couches avec des périodes de 40 à 80 Å et des empilements silicium/tungstène de 100 couches avec des périodes de 20 à 30 Å présentant de bonnes réflectivités.

Abstract. — Ellipsometry is a characterization method allowing the determination of the optical index and of the thickness of thin films. We have used this method to control, during their growth, the realization of diode RF sputtered soft X-ray multilayers. Three parameters limit the multilayer reflectivity : compactness defects, thickness drift and interface roughness. Our ellipsometers' accuracy being 0.1 Å on thickness and 10^{-3} on optical index, we have been able to optimize the deposit thickness, to control the growth rate and to understand the interface formation mechanism. This has enabled us to produce soft X-ray optics of good quality for wavelengths down to 44.7 Å. Thus C/W 200 layer stacks with period from 40 Å to 80 Å and Si/W 100 layer stacks with period from 20 Å to 30 Å showing good reflectivities have been achieved.

Introduction.

X-UV optics production [1-7] calls on well known deposit techniques of the optical visible range : evaporation, sputtering. Meanwhile X-UV multilayers need extremely low thickness (of the order of a nanometer) and a very high number of layers (about one hundred). The thickness has to be controlled to better than 0.1 Å and the interface roughness has to be less than 3 Å, and this all along the stack, to obtain significant reflectivities. So it appears essential to us to understand the physical way of growth of the ultra thin layers. In that way we have chosen to use *in situ* kinetic ellipsometry. Then we have adapted this method to a diode RF sputtering system devised for C/W and Si/W soft X-ray multilayer realization.

1. Ellipsometry.

1.1 PRINCIPLE. — Ellipsometry [7-14] consists of the analysis of the polarization of the light reflected by a sample, the light having been polarized initially in a known state. The difference in phases of the reflected light between the two polarizations, parallel (P) and normal (S) to the plane of incidence, is noted Δ and the attenuation ratio between p and s waves is noted $\tan \psi$. The couple $(\tan \psi, \cos \Delta)$ is characteristic of the dielectric function of the deposited layer and its thickness. Then we observe, in the $(\tan \psi, \cos \Delta)$ plane, trajectories corresponding to the growth of the deposited materials or stacks. Ellipsometry is very sensitive to the optical indexes contrast between deposit and substrate.

Then for a multilayer stack we always observe an important evolution of the point $(\tan \psi, \cos \Delta)$ whatever the number of realized layers may be (Fig. 2).

(*) LEP : a member of the Philips Research Organization.

1.2 EXPERIMENTAL SET UP. — Our sputtering system is equipped with two fixed targets. The sample moves alternately from a target to the other during the multilayer deposit. Fast shutters in front of the targets allow the sample to be uncovered very quickly (0.1 s).

The rotation direction of the screens is always the same. These two characteristics allow a very homogeneous deposit (3 inches). The distance between shutter and sample (few mm) is very low in regard to the target-sample distance (10 cm) to avoid strong perturbations of the plasma during the shutter opening. Argon pressure (5×10^{-3} Torr) and target RF power (100 Watts) are regulated.

This deposit system is equipped with two ellipsometers each recording one material growth. Each ellipsometer (Fig. 3) has a He-Ne source (6328 Å). The laser emitted light is polarized by a glan laser type fixed polarizer. After reflection on the sample, it is analysed by a rotating polarizer before reaching a photomultiplier. The analysis of the obtained sinusoidal signal allows the determination of $\tan \psi$ and $\cos \Delta$. The complete deposit system with the ellipsometer is controlled by a microcomputer.

2. Deposit quality.

2.1 OXIDATION. — When we open the vacuum chamber the tungsten target is oxidized. Then we observe tungsten trajectories different from those corresponding to pure tungsten (Fig. 4). We have to note that if we control with great accuracy the part of light element (C, O, vacuum) in a tungsten layer it is very difficult to determine what kind of element it is. We interpret the trajectories observed just after the chamber closing as corresponding to the deposit of the target surface oxide because these layers are obtained in conditions excluding any porosity in standard deposit. To avoid this oxide deposit we realize long pre-sputtering on a screen protecting the sample, up to the total cleaning of the target surface. Then we are able to deposit a good compactness of tungsten.

2.2 CONTAMINATION. — We can observe (Fig. 5) ellipsometric trajectories corresponding to different tungsten qualities. It starts from the same float-glass point and moves to the bulk tungsten accumulation point. Trajectory A corresponds to a good compacity tungsten ($\rho = 19.3 \text{ g/cm}^3$, $(n, k) = (3.8, 3.5)$). Trajectory B does not correspond to an oxidized layer nor to a porous layer. This trajectory is interpreted as a composition gradient of tungsten and silicon. As a matter of fact the layer starts with a W-Si mixing (50%/50%) to progressively evolve, after 200 Å growth, to pure tungsten.

This tungsten layer has been realized after long silicon thick film deposit. Then tungsten target had been covered with few ten angström of silicon.

During the first deposit of tungsten we have re-sputtered this silicon-tungsten mixed layer on our sample.

We have avoided this problem lighting together the two plasma under each target whatever the deposit may be : single layer or multilayer.

2.3 POROSITY. — Argon pressure value is very important for the layer quality. This is well shown on two examples. The first concerns tungsten growth. We can observe (Fig. 6) two trajectories corresponding to different tungsten growths. Trajectory A corresponds to low pressure deposited tungsten (5×10^{-3} Torr). The optical indexes determined are the tungsten ones. Grazing X-ray reflection analysis confirms the good compactness of this layer (19.3 g/cm^3) corresponding to pure homogeneous tungsten. Trajectory B corresponds to high pressure deposited tungsten (10^{-2} Torr). This growth simulation corresponds to porous tungsten (65 % W/35 % vacuum).

The second example concerns carbon growth. The same effect is observed (Fig. 7). At low pressure (4.5×10^{-3} Torr) we deposit pure carbon (trajectory A) and at high pressure (10^{-2} Torr) porous carbon (trajectory B).

In the two cases we can understand this compactness difference *versus* pressure in « ion plating » term. As a matter of fact at low pressure the high value of the mean free path allows the sputtered material atoms and the neutralized argon ions retrodiffused by the target to reach the sample with enough energy to cram the layer during its growth and then to obtain optimal density.

This phenomenon is inhibited at high pressure. The important collision number before reaching the sample surface does not allow this densification process. Then we always sputtered at low pressure to obtain optimal density layer with a good reproducibility.

3. Layer thickness.

We can observe figure 8 the ellipsometric trajectory corresponding to a carbon layer growth. At constant pressure (4.5×10^{-3} Torr) we suddenly have changed the RF power from 400 Watts to 600 Watts. Then we observe an immediate increase of the growth rate from 0.3 Å/s to 0.6 Å/s. We can note that this rate variation is observed without any significant optical index variation. We observe the same phenomenon for the silicon. Figure 9 shows two trajectories corresponding to two silicon growth realized at 200 Watts and 400 Watts. The growth rates are 0.3 Å/s and 1.6 Å/s. As for carbon we do not observe any significant composition variation from one layer to the other. An RF power increase gives a growth rate increase without deposit quality variation. As a matter of fact the flow increase of the

sputtered atoms reaching the sample induces a growth rate increase. On the other hand the energy increase of the sputtered atoms and of the neutralized ions retrodiffused by the target, which could increase the bombardment of the sample at high power, is compensated in this case by the plasma densification. Then ions and atoms reaching the sample have about the same energy at high and low power. So we do not observe any deposition compactness variation *versus* the RF power.

Then we have access to one parameter essentially acting on the growth rate. We have a great choice in the rate. To facilitate the ellipsometric control of the growth we have chosen to deposit at low power (50 Watts for tungsten, 100 Watts for silicon, 200 Watts for carbon). Then we obtain growth rate of about 0.2 Å/s allowing thickness accuracy control of about 0.1 Å using ellipsometry. We have been able to observe with a great accuracy the formation of the different interfaces in the multilayers.

4. Interface roughness.

4.1 CARBON-TUNGSTEN INTERFACES. — We can observe (Fig. 10) the ellipsometric trajectory of the interface corresponding to the growth of a tungsten layer (20 Å) on a carbon one (20 Å). This interface is very abrupt and the ellipsometric simulation with an optical index gradient (from carbon (2.03, 0.18) to tungsten (3.8, 3.5)) gives 1.5 Å roughness value. Different reasons can explain this low value. As a matter of fact, carbon has a compact amorphous structure (no microcrystals observed in electron diffraction) with a very low surface roughness (0 to 2 Å). Dissociation energy of the carbon atoms (100 to 200 kcal/mole) is very superior to the energy of the tungsten atoms reaching the sample. Then tungsten can be implanted neither deeply nor in great quantity in the carbon layer. Only few argon ions (less than 0.1 %) neutralized and retro-diffused by the target are found in the carbon layer.

Then the tungsten is deposited on a smooth and strong surface on which it is easily caught due to the low formation enthalpy (10 kcal/mole) of the tungsten carbide. Using ellipsometry we observe the filling of the carbon surface layer with the tungsten atoms. We progressively pass from a carbon-vacuum layer to a carbon-tungsten one (ellipsometry being very sensitive as shown Sect. 1.1). Then we observe the growth of tungsten on tungsten.

4.2 TUNGSTEN-CARBON INTERFACES. — Figure 11 presents the interface corresponding to the growth of a carbon layer (20 Å) on a tungsten one (20 Å). In a first time we observe the signal stagnation (20 s \leftrightarrow 5 Å carbon) then the deposit starts. We can explain this phenomenon because of the tungsten layer structure. As a matter of fact tungsten presents

beyond the coalescence thickness (8 to 10 Å) a microcrystalline structure as we can see on the electronic diffraction pattern (photos 1a et 1b). The microcrystals puzzled are separated by « grain boundaries » or amorphous zone. Then the tungsten surface roughness is higher (2 to 4 Å) than the carbon one. The carbon atoms are implanted in the tungsten by diffusion in the boundaries or they are retrodiffused. During this phase, the carbon smooths the tungsten roughness filling the tungsten surface layer defects. Then we pass from a tungsten-vacuum surface layer to a tungsten-carbon surface layer. Carbon having an optical index (2, 0.15) near the vacuum one for 6328 Å wavelength, we do not observe any evolution of the ellipsometric point during the smoothing. When the smoothing is finished we observe abruptly the start of the carbon growth on carbon. Simulation of this interface gives roughness value of about 3 Å.

4.3 TUNGSTEN-SILICON INTERFACES. — We observe the same smoothing process of the tungsten layer during the silicon deposit. As a matter of fact, as with the carbon atoms, the silicon ones fill up the tungsten asperity and diffuse in the surface layer. However, contrary to the carbon, the silicon having an optical index (4.7, 0.65) very different from the vacuum one at 6328 Å, the progressive passage from a tungsten-vacuum surface layer to a tungsten silicon interface layer is very visible with the ellipsometric measurement. We observe (Fig. 12) in a first time the silicon diffusion in the tungsten the signal slow moving (stagnant points), then a mixing phase between silicon and surface tungsten and finally the silicon growth on silicon. The roughness value of this interface is about the same as the tungsten-carbon one (3 Å).

4.4 SILICON-TUNGSTEN INTERFACES. — The silicon-tungsten interface formation (Fig. 13) is very different from the carbon-tungsten one. As a matter of fact the carbon surface is very smooth and strong because of the carbon properties. Silicon presents a rougher surface and especially has a very low dissociation energy (40 kcal/mole) in regard to the carbon one. The tungsten atoms and the neutralized argon ions retro-diffused by the target could be easily implanted in the silicon layer and could easily perturb the surface layer. This restructuration is all the more easy because the tungsten silicide formation enthalpy is low (5 kcal/mole). After the erosion and the implantation (phase B) we observe with ellipsometry the growth of a surface layer whose composition involves up to tungsten saturation (phase C). Then we observe the tungsten growth on tungsten (phase D). This interface is more diffuse than the carbon-tungsten one and presents roughness value of about 5 Å.

5. Soft X-ray multilayers.

In situ kinetic ellipsometry has allowed us to understand the growth process of the materials constituting the soft X-ray multilayers. Then we have been able to develop our deposition chamber and to find good deposit conditions (low pressure, low RF power). The use of ultra-high vacuum technology, of a very performant pump and a lock chamber gives a very great cleanliness in the sputtering chamber. Screens and caches protect targets and samples from all pollution. Fast shutters covering and uncovering the sample allow a very great accuracy on the deposited thicknesses. RF power and argon pressure regulation systems give a very great reproductibility of the deposit. The complete system is controlled by a microcomputer. The thickness accuracy is about 0.03 %. This accuracy being better than the ellipsometry one (0.2 %) we have not used ellipsometry as control system of soft X-ray multilayers realization but just as a method to understand the deposit processes.

The great intrinsic accuracy of the deposit system has allowed us to realize stacks with great number of layers (up to 200) and with low period (down to 20 Å). Then for C/W couple (Fig. 14) we obtain 17 % reflectivity ($K\alpha C$ 44.7 Å) for the sample 71 shown photos 2 and 3.

In the same way the W/Si couple seems promising as the first grazing X-ray reflection (1.54 Å) results shown figure 15 indicates.

6. Conclusion.

In situ kinetic ellipsometry, from its great thickness accuracy (0.1 Å) and its great optical index accuracy (0.1 %), has been proved an excellent method to characterize the growth of ultra thin layer (nanometer) stacks. We have been able to evidence the process of oxidation, contamination, porosification of the layer and to control the growth rate and at last to observe the interface formation. Then we have been able to propose models for the interface formation and to calculate the interfacial roughness. Ellipsometry has allowed us to optimize the X-ray multilayer deposit conditions and then to realize W/C and W/Si stacks with good reflectivities.

Acknowledgments.

I would like to thank Mr. V. Bodart (LEP) and Mr. J. A. Sirat (LEP) for their contributions to the ellipsometric measurements, Mr. Barchewitz (Chimie Physique Université Paris 6) for the soft X-ray reflection data, Mr. C. Schiller (LEP) for the grazing X-ray reflection data and Mr. P. Ruterana (LEP) for the T.E.M. micrographs.

References

- [1] BARBEE, T. W., Application of thin film multilayered structures of figured X-ray optics (San Diego) *SPIE* **563** (Août 1985) 2.
- [2] SPILLER, E., Application of thin film multilayered structures to figured X-ray optics (San Diego) *SPIE* **563** (Août 1985) 135.
- [3] FALCO *et al.*, Application of thin film multilayered structures to figured X-ray optics (San Diego) *SPIE* **563** (Août 1985) 195.
- [4] DHEZ, P. *et al.*, Projet de rapport de fin de contrat SGDN, ERA 719 et LURE (Mai 1985).
- [5] HOUDY, Ph. *et al.*, International Conference on Soft X-ray Optics and Technology (Berlin, RFA) *SPIE* **733** (Décembre 1986).
- [6] ZIEGLER, E., Application of thin film multilayered structures to figures X-ray optics (San Diego) *SPIE* **563** (Août 1985) 306.
- [7] BODART, V., Thèse, Université Paris 7 (1987).
- [8] AZZAM, R. M. A., BASHARA, N. M., Ellipsometry and Polarized Light (North Holland, Amsterdam) 1977.
- [9] ASPNES, D., *J. Phys. Colloq. France* **44** (1983) C10-610.
- [10] THEETEN, J. B. *et al.*, *Acta Electron.* **21** (1978) 231.
- [11] ERMAN, M., Thèse de Docteur ès-Science, Université Paris 6 (1986).
- [12] DREVILLON, *Rev. Sci. Instrum.* **53** (July 1982).
- [13] HOUDY, Ph. *et al.*, *Thin Solid Film* **141** (1986) 99-109.
- [14] BODART, V. *et al.*, Proc. SFV Int. Symp. on Trends and New applications in Thin Films (Strasbourg) **1** (Mars 1987) 15.

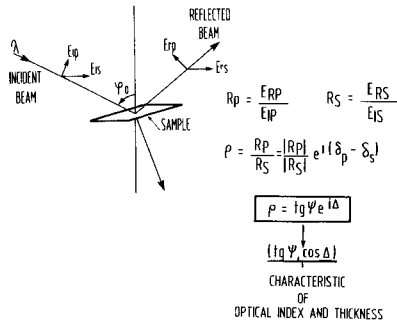


Fig. 1. — Ellipsometry principle.

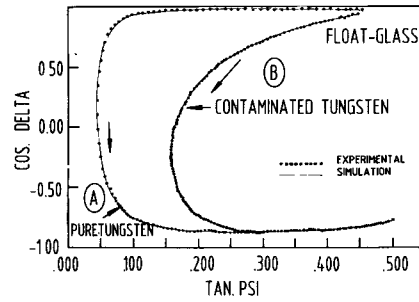


Fig. 5. — Trajectories for two different tungsten qualities : pure one and contaminated one.

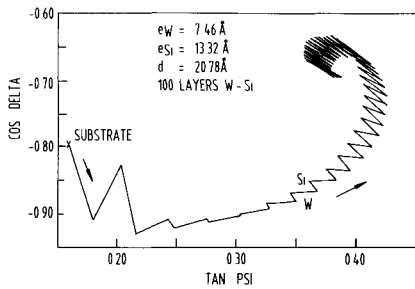


Fig. 2. — Experimental trajectory of a W/Si multilayer.

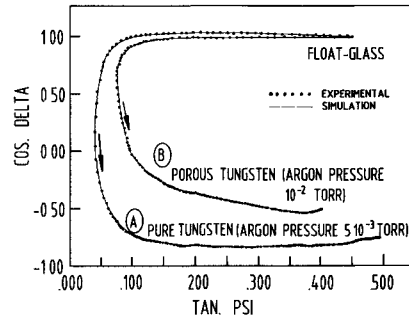


Fig. 6. — Trajectories for two different tungsten qualities : compact one and porous one.

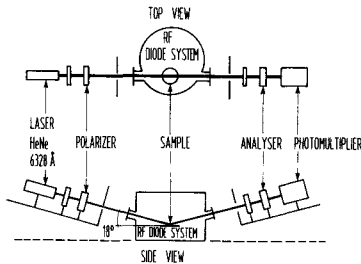


Fig. 3. — Schema of an *in situ* ellipsometer.

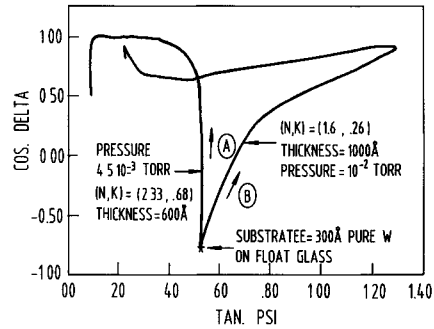


Fig. 7. — Trajectories for two different carbon qualities : compact one and porous one.

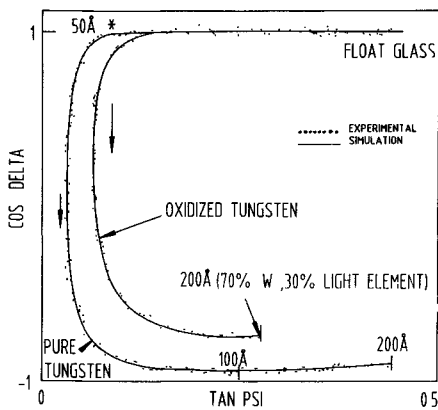


Fig. 4. — Trajectories for two different tungsten qualities : pure one and oxidized one.

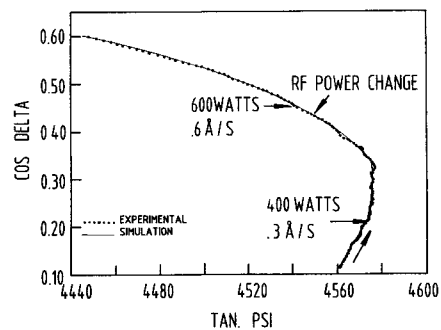


Fig. 8. — RF power change effect on growth rate of carbon layer.

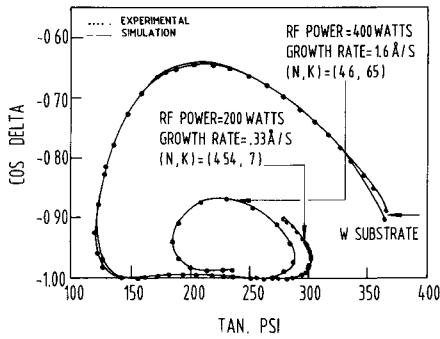


Fig. 9. — RF power effect on silicon growth.

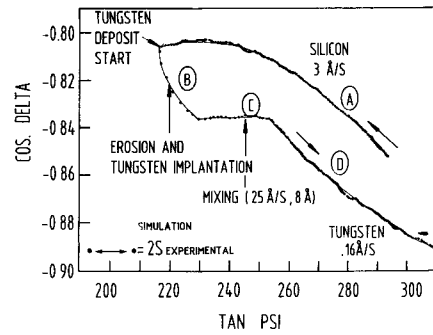


Fig. 13. — Interface corresponding to the growth of a tungsten layer on a silicon one : a) pure silicon growth ; b) erosion and tungsten implantation ; c) tungsten silicide formation and mixing ; d) pure tungsten growth.

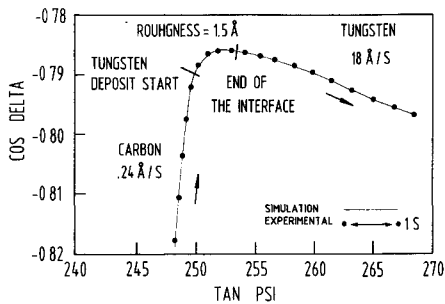


Fig. 10. — Interface corresponding to the growth of a tungsten layer on a carbon one.

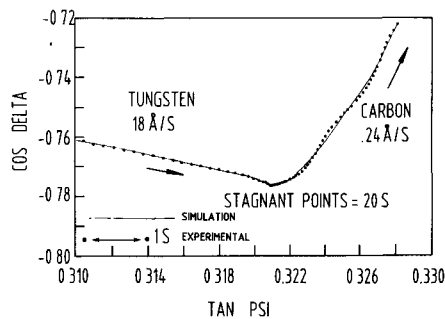


Fig. 11. — Interface corresponding to the growth of a carbon layer and a tungsten one.

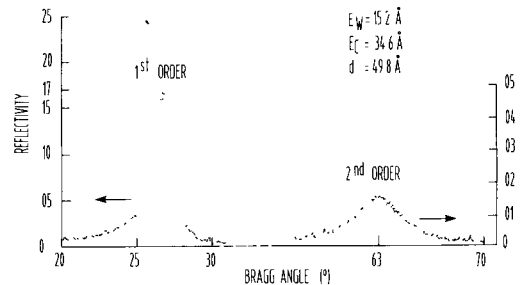


Fig. 14. — Absolute soft X-ray reflectivity (44.7 Å) of C-W stack (180 layers) sample 71.

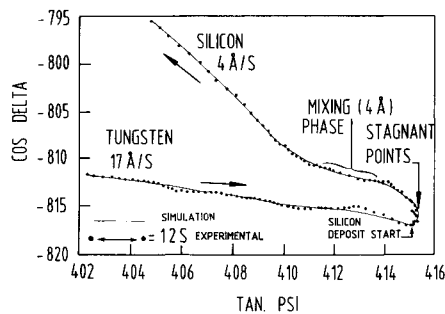


Fig. 12. — Interface corresponding to the growth of a silicon layer on a tungsten one.

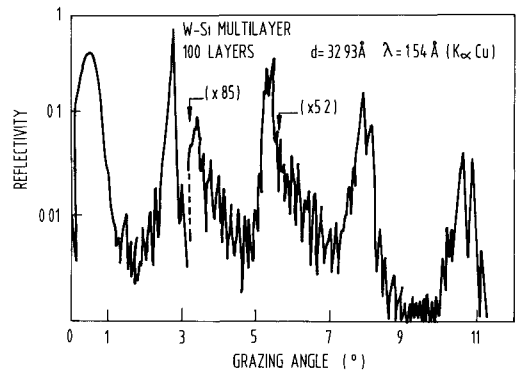


Fig. 15. — Grazing X-ray (1.54 Å) reflection of a W-Si multilayer (100 layers).

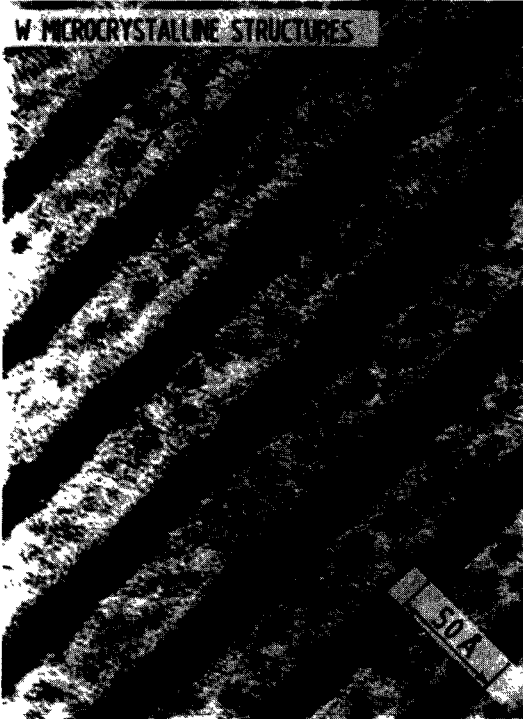


Photo 1A. — T.E.M. micrograph showing tungsten micro-crystals.

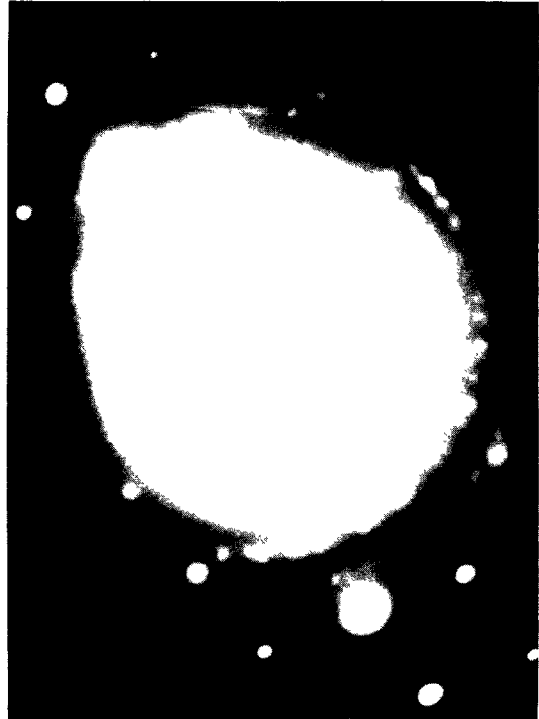


Photo 1B. — Electron diffraction image of a W-C multilayer showing tungsten micro-crystals.

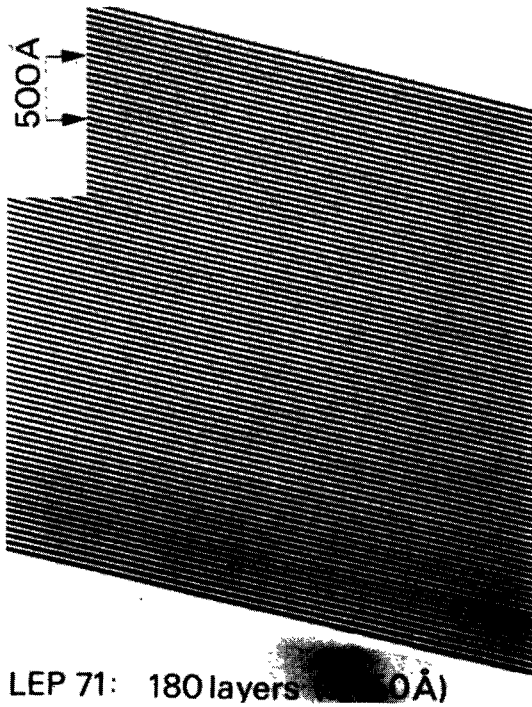


Photo 2. — T.E.M. micrograph of the sample 71.

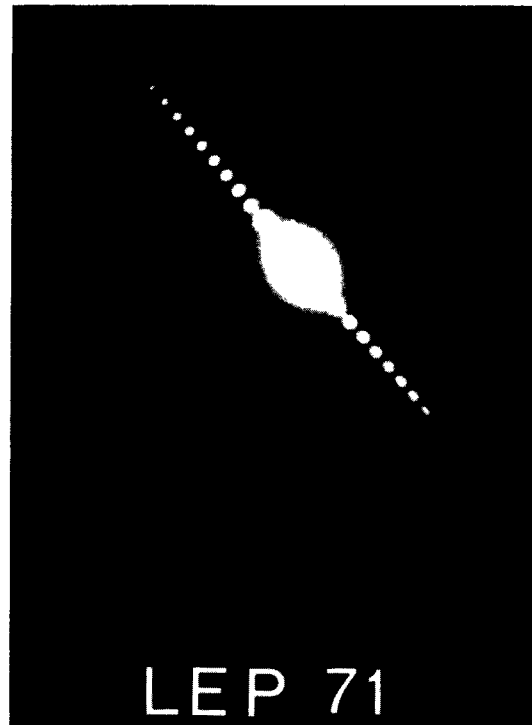


Photo 3. — T.E.M. diffraction of the sample 71.